Nanotoxicology, 2011; Early Online, 1–11

ISSN: 1743-5390 print / 1743-5404 online
DOI: 10.3109/17435390.2011.635814

informa
healthcare

Quantum dot 705, a cadmium-based nanoparticle, induces persistent inflammation and granuloma formation in the mouse lung

Chia-Chi Ho[1,2], Han Chang[3,4], Hui-Ti Tsai[2], Ming-Hsien Tsai[2], Chung-Shi Yang[5], Yong-Chien Ling[1,6], & Pinpin Lin[2]

[1]Institute of NanoEngineering and Microsystems, National Tsing Hua University, Hsinchu, Taiwan, [2]Division of Environmental Health and Occupational Medicine, National Health Research Institutes, Zhunan, Taiwan, [3]Department of Pathology, China Medical University Hospital, Taichung, Taiwan, [4]Department of Pathology, School of Medicine, China Medical University, Taichung, Taiwan, [5]Center for Nanomedicine Research, National Health Research Institutes, Zhunan, Taiwan and [6]Department of Chemistry, National Tsing Hua University, Hsinchu, Taiwan

Abstract

Some quantum dots (QDs) have been applied for drug delivery and imaging in biological systems. Drug delivery via the lung and lung imaging are potential applications of QDs. QD705 is cadmium based. The aims of the study were to evaluate the biological effects of QD705 in the lungs and the protective effects of polyethylene glycol (PEG) coating against QD705-induced biological responses. Intratracheal instillation of QD705-COOH persistently induced acute neutrophil infiltration, followed by interstitial lymphocyte infiltration and a granulomatous reaction on days 17 and 90. QD705-COOH also induced gene expression of cytokines, chemokines and metalloproteinase 12 in lung tissues. Furthermore, QD705-COOH transiently reduced pulmonary function on day 17. Treatment with QD705–PEG induced similar inflammatory responses and reduced pulmonary function on day 17, but the granulomatous reaction disappeared by day 90 These data indicated that administration of QD705 via the lung caused adverse responses and PEG coating failed to prevent these effects.

Keywords: Quantum dots, lung granuloma, biomaterials, nanotoxicology

Introduction

Nanoparticles are products of nanotechnology and are of increasing interest because of their industrial and biological applications. Quantum dots (QDs) are nanoparticles defined as small semiconductor crystals with discrete quantum states that have different chemical compositions (e.g. CdSe, CdTe, InAs, GaN) with different properties. QDs are of special interest because they have great potential for use as drug delivery, diagnostic and imaging agents in biomedicine (Xing et al. 2006; Gao and Dave 2007; Zhang et al. 2008; Mulder et al. 2010; Obonyo et al. 2010).

QD705 is approximately 12–20 nm in diameter with a metalloid crystalline core (Cd/Se/Te) surrounded by a thin shell or cap of zinc sulphide (ZnS) (Dabbousi et al. 1997). QD705 emits stable near-infrared fluorescence that can be used for long-term, multiplexed and quantitative imaging and detection (Gao et al. 2008). The surface of QD705 can be coated for specific applications, such as fluorescence efficiency, solubility in biological media or bio-conjugation to antibodies for specific diagnostic and therapeutic purposes (Gao et al. 2004; Mulder et al. 2010).

QDs have been utilised as carriers for drug delivery. The core of QDs can serve as structural scaffolds, and imaging contrast agents and small-molecule hydrophobic drugs can be linked between the inorganic core and the amphiphilic polymer-coating layer (Qi and Gao 2008). For example, Chen et al. (2005) reported a delivery approach by co-transfection of small interfering RNA and QDs. Manabe (2006) conjugated the QD surface with captopril, an antihypertensive drug, and studied its pharmacodynamics and pharmacokinetics in spontaneously hypertensive rats. Jia (2007) combined polyethyleneimine-coated carbon nanotubes with QDs for antisense oligodeoxynucleotide delivery.

Nanoparticles can be used to deliver drugs, genes or vaccines to specific tissues or cells by targeted delivery via the systemic route and non-invasive routes of administration, such as the pulmonary route. Drug delivery via the lung reduces drug metabolism and may enhance drug bioavailability. Liposomes in the nanometer range (Karathanasis et al. 2005; Gaspar et al. 2010) and nanoparticles (Zhang et al. 2009) exhibit some well-defined characteristics that have created an attractive and efficient approach for pulmonary delivery of drugs. Liposomes, such as bovactant

Correspondence: Pinpin Lin, Division of Environmental Health and Occupational Medicine, National Health Research Institutes, Zhunan, Taiwan. E-mail: pplin@nhri.org.tw. Yong-Chien Ling, Institute of NanoEngineering and Microsystems, National Tsing Hua University, Hsinchu, Taiwan and Department of Chemistry, National Tsing Hua University, Hsinchu, Taiwan. E-mail: ycling@mx.nthu.edu.tw

(Received 16 April 2011; accepted 18 October 2011)

(Alveofact® Dr Karl Thomae GmbH, Biberach, Germany), are one of the most extensively investigated systems for controlled delivery of drugs to the lung (Mansour et al. 2009). Solid lipid nanoparticles have been successfully applied as a pulmonary carrier system for insulin (Liu et al. 2008).

QDs with integrated targeting, imaging and therapeutic functions have become excellent materials to study drug delivery in cells and small animals. QDs have potential in biomedical applications, but concerns persist about their safety. Although many studies have reported toxicity of QDs *in vitro* (Lovric et al. 2005; Chan et al. 2006; Chang et al. 2006; Monteiro-Riviere et al. 2009; Mahto et al. 2010) and analysed the physiological behaviour of QDs (Deng et al. 2010), there are few studies of their biological and toxicity effects *in vivo* (Lin et al. 2008; Hauck et al. 2010; Lin et al. 2011).

Nanoparticle surface chemistry has been shown to influence toxicity *in vitro* (Ryman-Rasmussen et al. 2006). Ballou (2004) found that coating QDs with polyethylene glycol (PEG) molecules reduced accumulation in the liver and bone marrow. Several classes of protein drugs, such as enzymes, cytokines and antibodies, are coated with PEG with the advantages of a prolonged residence in the body, decreased degradation by metabolic enzymes and reduction or elimination of protein immunogenicity (Veronese and Pasut 2005). A QD coated with PEG can be further conjugated with bioactive moieties to target specific biologic events or cellular structural features.

In the present study, we evaluated the biological effects of QD705 on the lungs and the protective effects of PEG coating against QD705-induced biological responses in the mouse lung. Our findings provide important new insights regarding the use of CdSe-core QDs as drug carriers via the lung.

Methods

Nanoparticles

The QD705 nanoparticles used in our experiments were purchased from Invitrogen, Inc. (Hayward, CA, USA) as Qtracker 705 non-targeted QDs (QD705-PEG) and Qdot® 705 ITK™ carboxyl QDs (QD705-COOH).

QD705-PEG and QD705-COOH contain a Cd/Se/Te core covered with a ZnS shell, but only QD705-PEG is modified with a methoxy-PEG−5000 coating; QD705-COOH is modified with a carboxyl group. We used titanium dioxide (Degussa, P-25) powder obtained from Nippon Aerosil Co. Ltd. (Tokyo, Japan). The nano-TiO_2 contained anatase and rutile phases in a ratio of about 3: 1. The 30-nm nano-SiO_2 particles were amorphous silica and were purchased from Glantreo Ltd, Cork, Ireland.

Physicochemical characterisation of nanoparticles

Nanoparticles were characterised for size distribution, zeta potential, size and shape. The hydrodynamic diameters and zeta potentials of the nanoparticles were measured with the Zetasizer Nano system (Zetasizer Nano ZS, Malvern Instruments, Worcestershire, UK). Dynamic laser light scattering measurements were checked in a single-scattering regime with l = 633 nm at an angle of 173°. The suspension was put into a cuvette at 25°C to enable particle size and zeta potential analysis. The shape and size of the nanoparticles were assessed by transmission electron microscopy (TEM) (H-7650, Hitachi, Japan). The nanoparticle solution was then dripped on copper grids for TEM. All of the copper grids were preserved in a dry cabinet.

Cell culture

Mouse lung type II cell line MLE12 cells immortalised with SV40 (American Type Culture Collection, Manassas, VA, USA) were maintained in Dulbecco's Modified Eagle's Medium/Nutrient Mixture F-12 Ham (Sigma-Aldrich™, New York, USA) with 2.5 mM L-glutamine, 10 mM HEPES, 1.5 g/l sodium bicarbonate and 2% FBS. Mouse macrophage J774A.1 cells derived from BALB/c mice (American Type Culture Collection, Manassas, VA, USA) were maintained in Dulbecco's Modified Eagle's Medium (GIBCO™) with 4 mM L-glutamine, 1.5 g/l sodium bicarbonate, 2.38 g/l glucose and 10% FBS. MLE12 and J774A.1 cells were incubated in a 37°C incubator with a humidified mixture of 5% CO_2 and 95% air. The medium was changed twice a week, and cells were passaged by trypsinisation every week.

Cytotoxicity assay

Cytotoxicity of QD705-PEG, QD705-COOH, TiO_2 and SiO_2 was determined with dimethylthiazoldiphenyltetrazolium bromide (MTT) assay. MLE12 cells (3000 per well) and J774A.1 cells (5000 per well) were seeded in 96-well plates for 24 h and then incubated with vehicle (1% borate buffer, 1% mouse serum albumin and 1% double-distilled water (ddH_2O)), QD705-PEG, QD705-COOH, TiO_2 and SiO_2 for 48 h. Subsequently, 1 mg/ml MTT was added to the medium and cells were incubated for an additional 4 h. Precipitated formazan was dissolved in 0.2 ml DMSO and the absorbance was measured at 535 nm. The data are presented as the percentage of controls. All vehicles, including 1% borate buffer, 1% mouse serum albumin and 1% ddH_2O, had no significant cytotoxicity.

Colony formation assay

This method was used for assessing long-term cytotoxicity. Cells were seeded on 6 cm dishes for 24 h and then incubated with vehicle, QD705-PEG or QD705-COOH for 24 h. Then, cells were reseeded on 6-well plates and incubated with fresh media. After incubation for 7 days, adherent cells were washed twice with PBS, fixed with 100% ethanol for 20 min at room temperature. The colonies were stained with 10% Giemsa solution for 30 min, then washed with water and air-dried. The experiment was performed in triplicate.

Animals and animal treatment

Six-week-old male ICR mice were purchased from Bio-LASCO (Taipei, Taiwan) and acclimated for 2 weeks in the animal facilities at the National Health Research Institutes (NHRI). All animal treatments and experimental protocols

for this study were reviewed and approved by the Institutional Animal Care and Use Committee at NHRI. All mice were housed under a 12-h light/dark cycle, at 23 ± 1°C, with a 39–43% relative humidity. Water and food were provided *ad libitum*. Eight mice (n = 8) per time point were randomly selected for experimentation. Each mouse was exposed via intratracheal instillation to a single dose of 60-μg QD705-PEG in borate buffer, 60-μg QD705-COOH in 0.03% mouse serum albumin (Sigma, New York, USA), 500-μg TiO_2 in ddH_2O or 100-micro-g SiO_2 in 0.03% mouse serum albumin; the injection volume was 30 μl/mouse. Serial sacrifices were carried out on days 2, 17 and 90. Isolation of lung lavage, measurement of pulmonary function and histopathological evaluation were done in the same animals.

Preparation and evaluations of bronchoalveolar lavage fluids

Animals were sacrificed via isoflurane inhalation to ensure that there was no undue suffering. The whole lung was dissected out surgically and was lavaged with 1 ml saline. The recovered amount of lavagate was recorded and saved in individually labelled bottles. The total cell numbers and cell types in the bronchoalveolar lavage fluid (BALF) from the animals were determined with a cell counter (Coulter Inc., Miami, FL, USA). The BALF was centrifuged at 800 g for 15 min using a Shandon Cytospin 4 (Thermo Scientific, Waltham, MA, USA). The cytospin smear was then prepared and Liu's staining (Tonyar Biotech, Tao Yuan, Taiwan) was performed to distinguish different cell types. Cells in the BALF were classified into three main categories, non-viable cells, epithelial cells and leucocytes (including macrophages, neutrophils and lymphocytes).

Total protein and lactate dehydrogenase activity in the BALF

Measurement of total protein in the BALF supernatant was performed by Bradford assay (Bio-Rad, Hercules, CA, USA) with bovine serum albumin as a standard. The activity of lactate dehydrogenase (LDH) was spectrophotometrically assayed using the CytoTox96 Non-Radioactive Cytotoxicity assay (Promega Corporation, Madison, WI, USA) at 490 nm in the presence of lactate.

Histopathology and localisation of QD705

Formalin-fixed and paraffin-embedded lung tissues were serially sectioned at 3-μm thickness with a rotary microtome. Haematoxylin and eosin (H&E) were used for general histology staining in accordance with standard H&E staining procedures. QD705 was detected as red fluorescent particles under the fluorescence microscope.

Pulmonary function analysis

All mice were anesthetised, tracheostomised and placed in a forced pulmonary manoeuvre system (Buxco Research Systems©, Wilmington, North Carolina, USA). Three semi-automatic manoeuvres were used in the Buxco system, the Boyle's law functional residual capacity (FRC), quasi-static pressure–volume and fast flow volume manoeuvre. The FRC was determined according to Boyle's law with Boyle's law FRC. With the quasi-static pressure–volume manoeuvre, total lung capacity (TLC), residual volume (RV) and vital capacity (VC) were recorded. To measure forced expiratory flow (FEF) and peak expiratory flow and forced expiratory volumes such as forced vital capacity (FVC) and forced expiratory volume at 100 msec (FEV100), the fast flow volume manoeuvre was performed. These tasks must be automated and parameters calculated on line using a personal computer in an easy-to-use, all-inclusive system.

Quantitative real-time reverse transcription–polymerase chain reaction assay

Tissues (n = 8) soaked in RNAlater solution (Ambion Inc., Austin, TX) were incubated at 4°C overnight and then transferred to a −80°C environment until RNA purification. Tissues were ground with a tissue homogeniser (MM301, Retsch Technology GmbH, Haan, Germany) in TRIZOL reagent (Life Technologies, Rockville, MD, USA), and then total RNA was purified via chloroform extraction. Synthesis of cDNA was performed using the High-Capacity cDNA Archive kit (P/N4322171, Applied Biosystems, Foster City, CA, USA) with 3.0-μg total RNA. Quantitative polymerase chain reaction was carried out using the TaqMan Universal PCR Master Mix (Applied Biosystems, Foster City, CA, USA) and analysed on StepOne™ and StepOnePlus™ PCR Systems (Perkin-Elmer Applied Biosystems, Foster City, CA, USA). The primers and probes for *tumour necrosis factor-alpha (TNF-α), interleukin-1 beta (IL-1β), interleukin-6 (IL-6), interleukin-10 (IL-10), interleukin-13 (IL-13), monocyte chemotactic protein-1 (MCP-1), chemokine (C-C motif) ligand 1 (*CCL1*), chemokine (C-C motif) ligand 17 (*CCL17*), chemokine(C-X-C motif) ligand 1 (CXCL1), chemokine (C-X-C motif) ligand 13 (CXCL13), matrix metalloproteinase-12* (*MMP-12*) and *glyceraldehyde-3-phosphate dehydrogenase (GAPDH)* were included in the Assay-on-Demand Gene Expression Assay Mix (Applied Biosystems). The PCR program was 95°C for 10 min followed by 40 cycles of 60°C for 1 min with 95°C for 15 sec. Quantitative values were obtained from the threshold cycle (C_T) number. The target gene expression level was normalised to glyceraldehyde 3-phosphate dehydrogenase (*GAPDH*) mRNA expression in each sample. The relative mRNA levels of the target gene = $2^{-\Delta Ct}$, $\Delta Ct = Ct_{\text{target gene}} - Ct_{GAPDH}$.

Statistical analysis

Comparison of the results between various experimentally treated groups and their corresponding controls was carried out by Student's t-test. All comparisons were considered significantly different when $p < 0.05$.

Results

Physicochemical properties of nanoparticles

The shape and size of nanoparticles were characterised by TEM and dynamic light scattering (DLS) (Figure 1, Table I). QD705-PEG and QD705-COOH were spherical nanoparticles with core sizes of 10.2 and 9.6 nm, respectively. Both

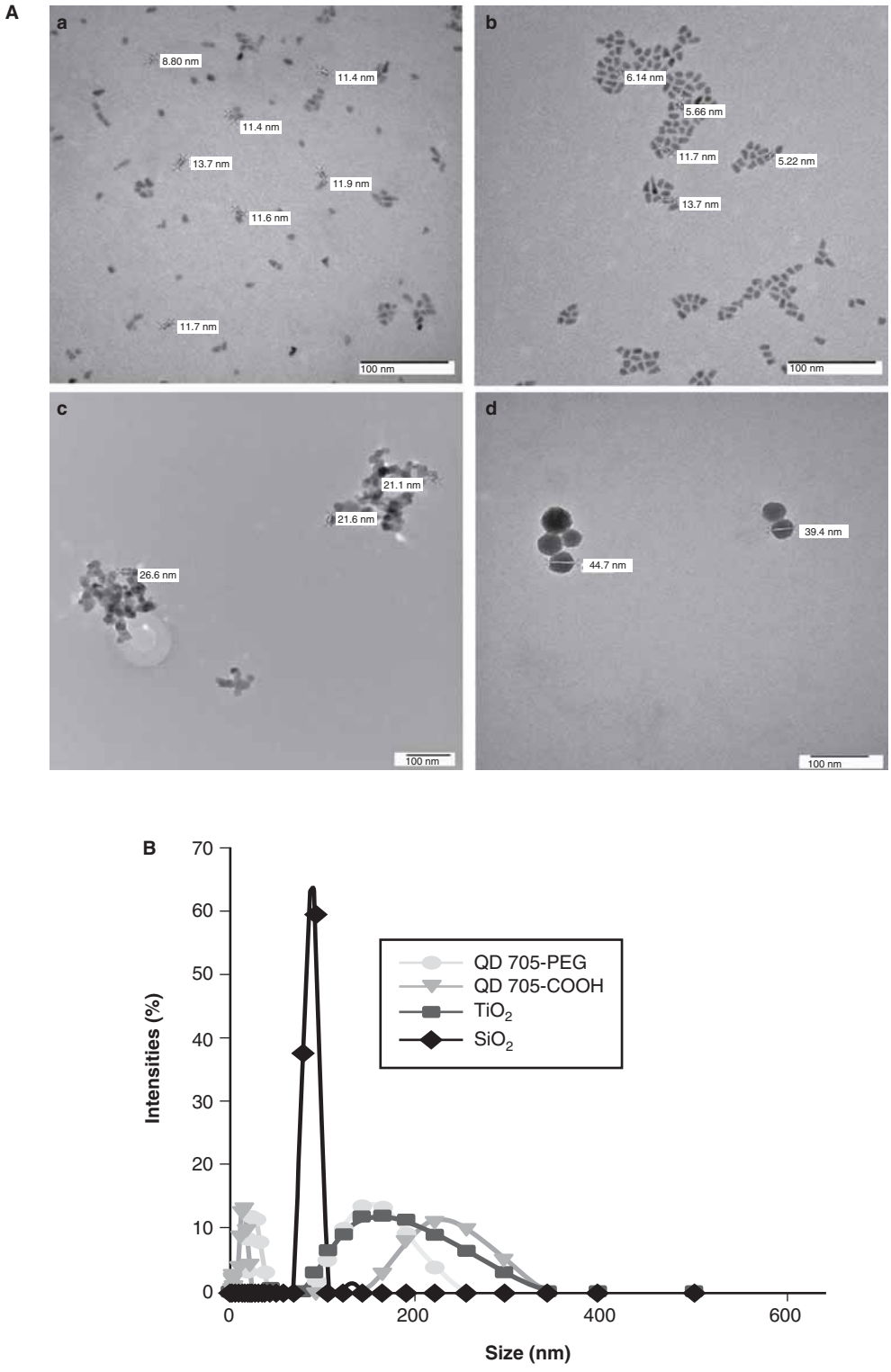

Figure 1. Sizes and shapes of nanoparticles. A. Transmission electron microscopy images: (a) QD705-PEG, (b) QD705-COOH, (c) TiO_2 and (d) SiO_2. B. Size distribution by dynamic light scattering.

QD705-PEG and QD705-COOH were partially aggregated in vehicle for the following animal studies (Figure 1). TiO_2 was 21.7 nm, but tremendously aggregated to 132 nm in water. SiO_2 with a 40.2-nm diameter aggregated to 86.4 nm in 0.03% mouse serum albumin. As shown in Table I, the zeta potential of QD705-PEG, QD705-COOH and SiO_2 were negative, but TiO_2 was positive.

Cytotoxicity of nanoparticles in mouse macrophages and lung type II cells

Macrophages and pneumocytes are two major cell types in lung tissues. For short and long-term cytotoxic effects, QD705-COOH was highly cytotoxic to mouse macrophage J774A.1, but only slightly cytotoxic to mouse type II pneumocyte MLE12 cells (Figure 2A, Figure 2B, Figure 2E

Table I. Physicochemical characterisation of the nanoparticles.

	Inorganic	Surface structure	Vehicle	Particle size (DLS) (nm)	Size (TEM) (nm)	Zeta potentials (mV)
QD705-PEG	Cd/Te/Se	PEG	Borate buffer, pH 8.3	26.6 nm, 152.7 nm (143.3)	10.2 ± 1.8 nm	-6.4 ± 0.6 mV
QD705-COOH	Cd/Te/Se	COOH	0.03% mouse serum albumin in water	14.3 nm, 295.9 nm (141.5)	9.6 ± 1.8 nm	-22.7 ± 0.4 mV
TiO_2	TiO_2	-	water	132.2 nm	21.7 ± 5.8 nm	31.2 ± 6.4 mV
SiO_2	SiO_2	-	0.03% mouse serum albumin in water	86.4 nm	40.2 ± 6.1 nm	-39.4 ± 4.0 mV

and Figure 2F). Consistent with cytotoxicity, cellular uptake of QD705-COOH was more obvious than that of QD705-PEG in J774A.1 cells (Insert in Figure 2A). However, QD705-PEG only slightly reduced cell viability in both J774A.1 and MLE12 cells. Nano-SiO_2 and nano-TiO_2 were relatively not cytotoxic in either J774A.1 or MLE12 cells (Figure 2C and Figure 2D). These results indicated that QD705-COOH was more cytotoxic than QD-PEG, nano-SiO_2 and nano-TiO_2 in macrophage J774A.1 cells. Furthermore, macrophages might be susceptible when the lung is exposed to QD705-COOH.

Effects of nanoparticles on cell numbers and bio-indicators in mouse BALF

Cell numbers in BALF are indicators of lung inflammation. We found that intratracheal instillation of 60-μg QD705-PEG and QD705-COOH significantly increased the numbers of lymphocytes and neutrophils in BALF on days 2, 17 and 90 post-treatment (Table II). The efficiency of lavage fluid recovery was similar between control group and QD705-treated group (data not shown). Similar effects were observed in mice treated with a lower dose (12 μg) of QD705-PEG and QD705-COOH at day 17. The numbers of macrophages were transiently reduced on day 17 (Table II) and eosinophils were not detectable in the BALF (data not shown). Intratracheal instillation of TiO_2 and SiO_2 increased neutrophil numbers on day 17 post-treatment, but the increase was much lower than that induced by QD705 treatment (Table II).

LDH activity in BALF is an indicator of cytotoxicity in lung tissues, and the total protein level in BALF is an indicator of enhanced cellular permeability in the lung tissues. Intratracheal instillation of QD705-PEG and QD705-COOH significantly increased LDH activity and total protein concentrations in the BALF on days 2, 17 and 90 (Figure 3A and Figure 3B). By contrast, TiO_2 and SiO_2 slightly increased LDH activity, but failed to increase total protein concentrations (Figure 3A and Figure 3B). It appears that QD705-PEG and QD705-COOH induced a lung inflammatory response accompanied by cytotoxic effects from 2 to 90 days. TiO_2 and SiO_2 induced a relatively mild inflammatory response.

Effects of nanoparticles on pulmonary histopathology and function

In vehicle-treated control groups, the lung morphology was normal and no inflammation reaction was observed. Dramatic pathological changes in the 60-μg QD705-treated lung were observed by light microscopy with haematoxylin–eosin staining. QD705-COOH-treated lungs showed acute necrotising inflammation in some bronchioles, characterised by bronchiolar epithelial necrosis mixed with the majority of neutrophils and some lymphocytes on day 2. By contrast, QD705-PEG-treated lung showed slight lymphocytic infiltration but a lack of neutrophils around the peribronchiolar areas (Figure 4B-a and d). On day 17, both QD705-COOH and QD705-PEG induced an accumulation of alveolar macrophages in the alveolar spaces, which were mainly around the bronchioles (Figure 4B-b and e). Some poorly formed granulomas in the peribronchiolar areas and in the interstitium accompanied by an inflammatory mixture of neutrophils and lymphocytes were also identified (Figure 4B-b and e). It was a striking finding that QD705-COOH-induced granulomas persistently presented from 2 to 90 days, but QD705-PEG-induced granulomas disappeared and many macrophages were present in the alveolar spaces on day 90 post-treatment (Figure 4B-c and f). Neutrophil and lymphocyte infiltration was persistent in QD705-PEG- and QD705-COOH-treated lung on day 90. Neither bronchiolar nor interstitial fibrosis was identified. QD705-COOH was present in the lung parenchyma on fluorescence microscopy and located in the alveolar macrophages and granulomas on days 2, 17 and 90 post-treatment (Figure 4A). The localisation of QD705-PEG was similar to that of QD705-COOH on days 2 and 17. On day 90, granulomas in QD705-PEG-treated mice disappeared, but the fluorescence of QD705-PEG was still detected in some enlarged alveolar macrophages.

Pulmonary function was assessed on day 17 after treatment with 60-μg QD705-PEG or QD705-COOH. Several parameters were significantly reduced by QD705-PEG or QD705-COOH, including FVC, FEV100, VC and FEF (Table III). These changes suggested obstructive dysfunction of the lung. There was no difference in the measurements between QD705-PEG and QD705-COOH treatment. However, these reductions recovered by day 90 after treatment with the higher dose (60 μg) of QD705-PEG and QD705-COOH (data not shown). Treatment with the lower dose (12 μg) of QD705-PEG and QD705-COOH did not reduce pulmonary function parameters (data not shown).

Effects of nanoparticles on expression of cytokines and chemokines in mouse lung tissues

Several studies have demonstrated that the enhanced secretion of pro-inflammatory cytokines is an important factor in the initiation and perpetuation of inflammation in lung tissues (Meldrum et al. 1998; Ballou et al. 2004). Therefore, we examined gene expression of cytokines and chemokines in lung tissue (Table IV). These relative mRNA levels were

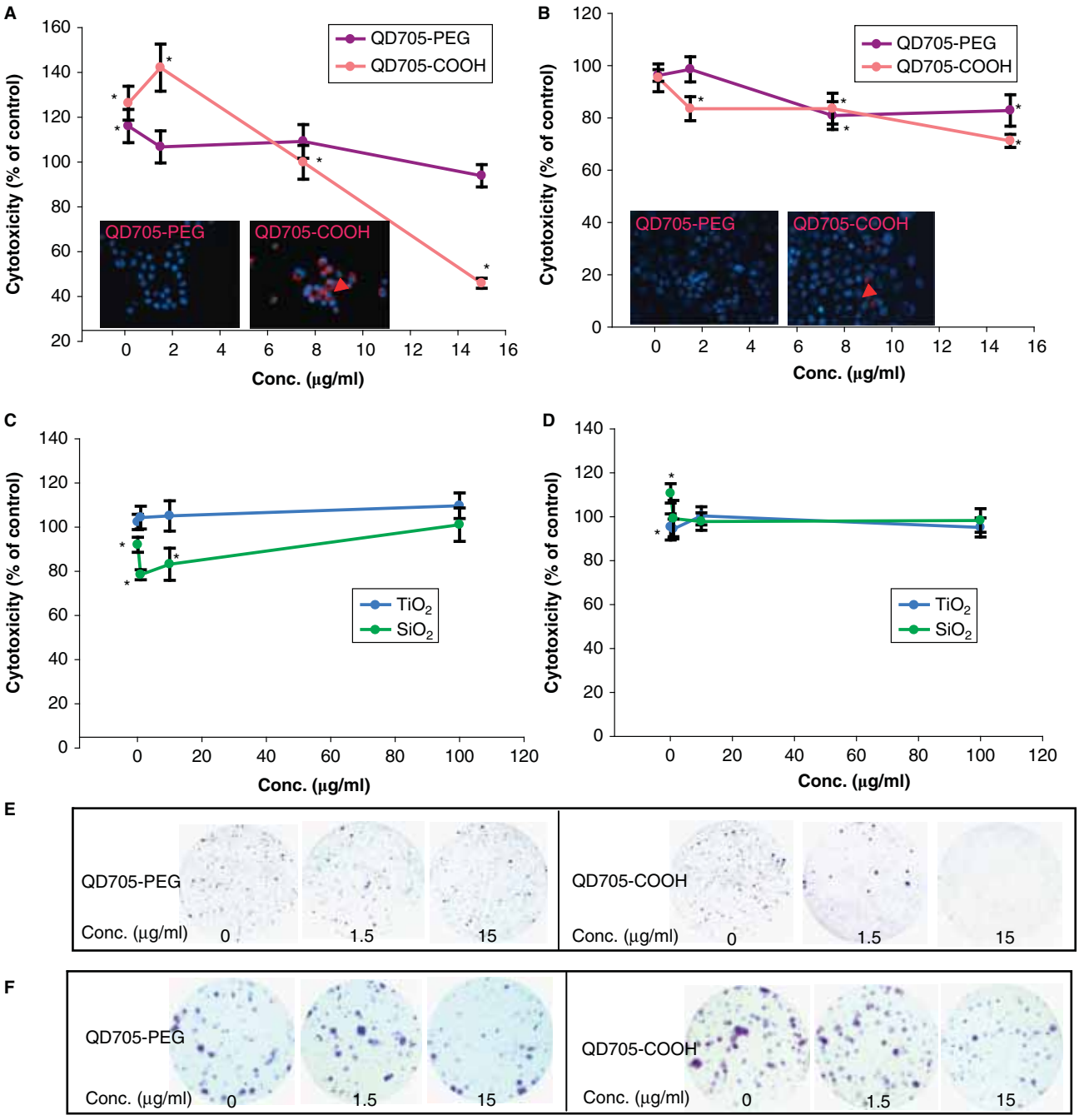

Figure 2. Cytotoxicity of nanoparticles in J774A.1 and MLE12 cells. (A) J774A.1 and (B) MLE12 cells were treated with QD705-PEG or QD705-COOH for 48 h. (C) J774A.1 cells and (D) MLE12 cells were treated with TiO_2 or SiO_2 for 48 h. Cell viability was determined with dimethylthiazoldiphenyltetrazolium bromide assay. Six samples were assayed in each experiment. Data are the mean ± SD for six independent experiments. *$p < 0.05$ compared with vehicle-treated cells. For colony formation assay, (E) J774A.1 and (F) MLE12 cells were treated with QD705-PEG or QD705-COOH for 24 h. Three samples were assayed in each experiment.

similar between borate buffer-treated group and mouse albumin-treated group. The mRNA levels of a battery of pro-inflammatory cytokines/chemokines, including TNF-α, IL-6, CXCL1 (KC) and MCP-1 (CCL2), were persistently elevated from day 2 to day 90 post-treatment with 60-μg QD705-PEG and QD705-COOH (Table IV). Treatment with the lower dose (12 μg) of QD705-PEG and QD705-COOH also increased pro-inflammatory cytokines/chemokines mRNA levels at day 17 post-treatment. However, SiO_2 did not have similar effects and TiO_2 only slightly increased TNF-α mRNA levels to 1.3-fold of control (Table IV). These data were consistent with histopathological changes; both QD705-PEG and QD705-COOH persistently induced inflammatory reactions in lung tissues.

IL-10 and IL-13 are classified as anti-inflammatory cytokines and reduce the secretion of pro-inflammatory cytokines by stimulated macrophages (Nathan and Denizot 1998). IL-10 and IL-13 mRNA levels were significantly elevated on day 17 with 12 and 60 μg of QD705-PEG and QD705-COOH, but only slightly with TiO_2. MMP-12 plays a pivotal role during tissue remodelling in pulmonary inflammatory diseases (Nenan 2005).We also found that

Table II. Total cell numbers and cell types in bronchoalveolar lavage fluid following nanoparticle treatment.

Treatment	Total cells	Cell number (*10^4)		
		Lymphocyte	Neutrophil	Macrophage
2 Days				
Borate buffer	5.97 ± 0.73	0.06 ± 0.04	0.08 ± 0.05	5.59 ± 0.89
60 μg QD705-PEG	9.91 ± 2.32*	0.16 ± 0.09*	1.97 ± 1.78*	6.81 ± 2.42
Mouse serum albumin	5.51 ± 1.22	0.04 ± 0.02	0.13 ± 0.05	4.37 ± 1.06
60 μg QD705-COOH	13.26 ± 4.16*	0.21 ± 0.06*	6.00 ± 3.25*	5.53 ± 2.22
17 Days				
Borate buffer	5.69 ± 2.64	0.02 ± 0.03	0.03 ± 0.01	5.06 ± 2.44
12 μg QD705-PEG	17.02 ± 4.18*	0.82 ± 0.57*	5.52 ± 3.56*	7.13 ± 2.66
60 μg QD705-PEG	11.29 ± 5.06*	2.11 ± 1.16*	4.62 ± 2.16*	2.56 ± 1.16*
Mouse serum albumin	8.40 ± 1.05	0.05 ± 0.03	0.03 ± 0.03	7.95 ± 0.75
12 μg QD705-COOH	26.57 ± 10.90*	2.08 ± 0.67*	10.74 ± 5.41*	6.84 ± 2.29
60 μg QD705-COOH	26.91 ± 1.37*	4.92 ± 3.83*	11.08 ± 6.54*	5.22 ± 1.94*
H_2O	6.69 ± 1.26	0.02 ± 0.02	0.02 ± 0.02	5.53 ± 1.20
500 μg TiO_2	6.62 ± 1.13	0.03 ± 0.03	0.07 ± 0.03*	4.83 ± 0.96
Mouse serum albumin	5.55 ± 1.75	0.05 ± 0.06	0.04 ± 0.03	6.24 ± 0.88
100 μg SiO_2	8.14 ± 2.12*	0.12 ± 0.09	0.11 ± 0.09*	5.96 ± 2.32
90 Days				
Borate buffer	7.61 ± 1.07	0.06 ± 0.06	0.06 ± 0.04	6.62 ± 1.00
60 μg QD705-PEG	25.90 ± 7.15*	1.74 ± 0.88*	7.74 ± 2.30*	8.68 ± 3.83
Mouse serum albumin	7.55 ± 1.39	0.08 ± 0.05	0.05 ± 0.05	6.62 ± 1.17
60 μg QD705-COOH	17.65 ± 3.12*	0.98 ± 0.29*	5.60 ± 3.05*	6.91 ± 2.53

Mice were given a single dose of nanoparticles via intratracheal instillation. Sacrifices were carried out at days 2, 17 and 90 after dosing. Each value represents the mean ± SD of eight mice. *$p < 0.05$ compared with the vehicle-treated group.

QD705-PEG and QD705-COOH time dependently increased MMP-12 mRNA levels. (Table IV) These results suggested that QD705-PEG and QD705-COOH induced lung remodelling on days 17 and 90 post-treatment.

The chemokines CCL1 and CCL17 are known to attract Th2 and regulatory T cells (Nakayama 2004). CXCL13 is one of the most important B-cell-attracting chemokines (Legler 1998). Treatment with 12 and 60 μg of QD705-PEG and QD705-COOH significantly increased CCL1, CCL17 and CXCL13 mRNA levels on day 17. While SiO_2 slightly increased CCL17 and CXCL13 expression, TiO_2 failed to induce chemokine expression. These data are consistent with lymphocyte infiltration after QD705-PEG and QD705-COOH treatment (Table IV).

Discussion

QDs are powerful fluorescent probes for long-term quantitative imaging, detection and drug delivery. Although drug delivery via the lung is an attractive application for QDs, the

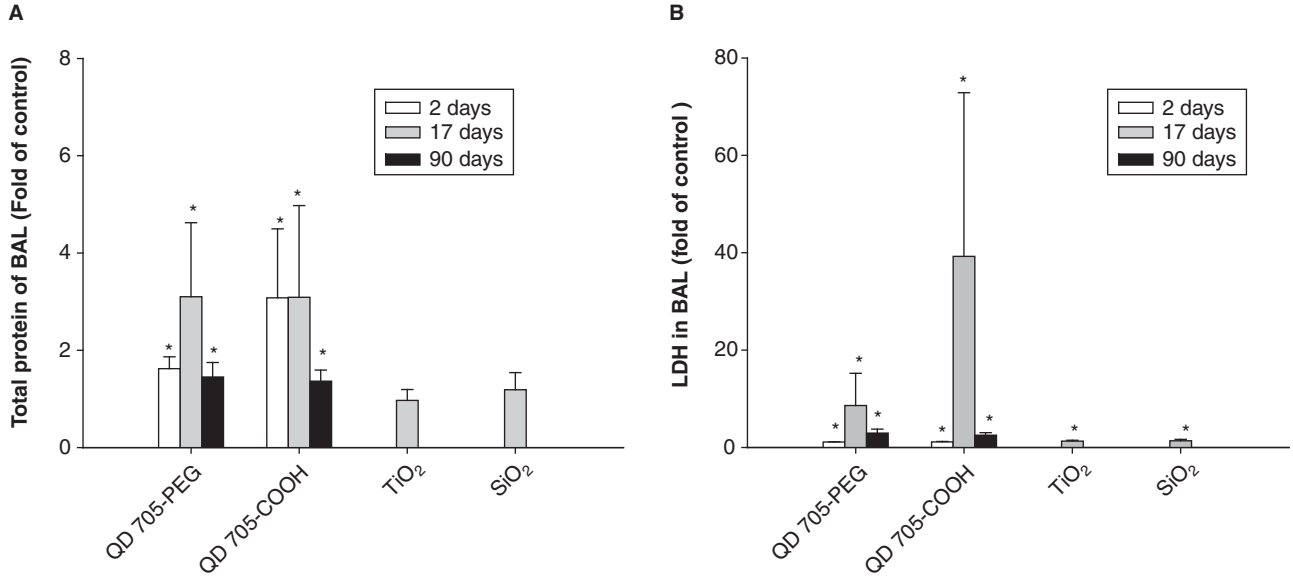

Figure 3. Protein concentration and lactate dehydrogenase (LDH) activity in bronchoalveolar lavage fluid (BALF) following nanoparticle treatment. (A) Total protein concentrations and (B) LDH released into the BALF following exposure to nanoparticles. Eight mice were assayed in each experiment. Data are the mean ± SD for eight independent experiments. *$p < 0.05$ compared with vehicle-treated cells.

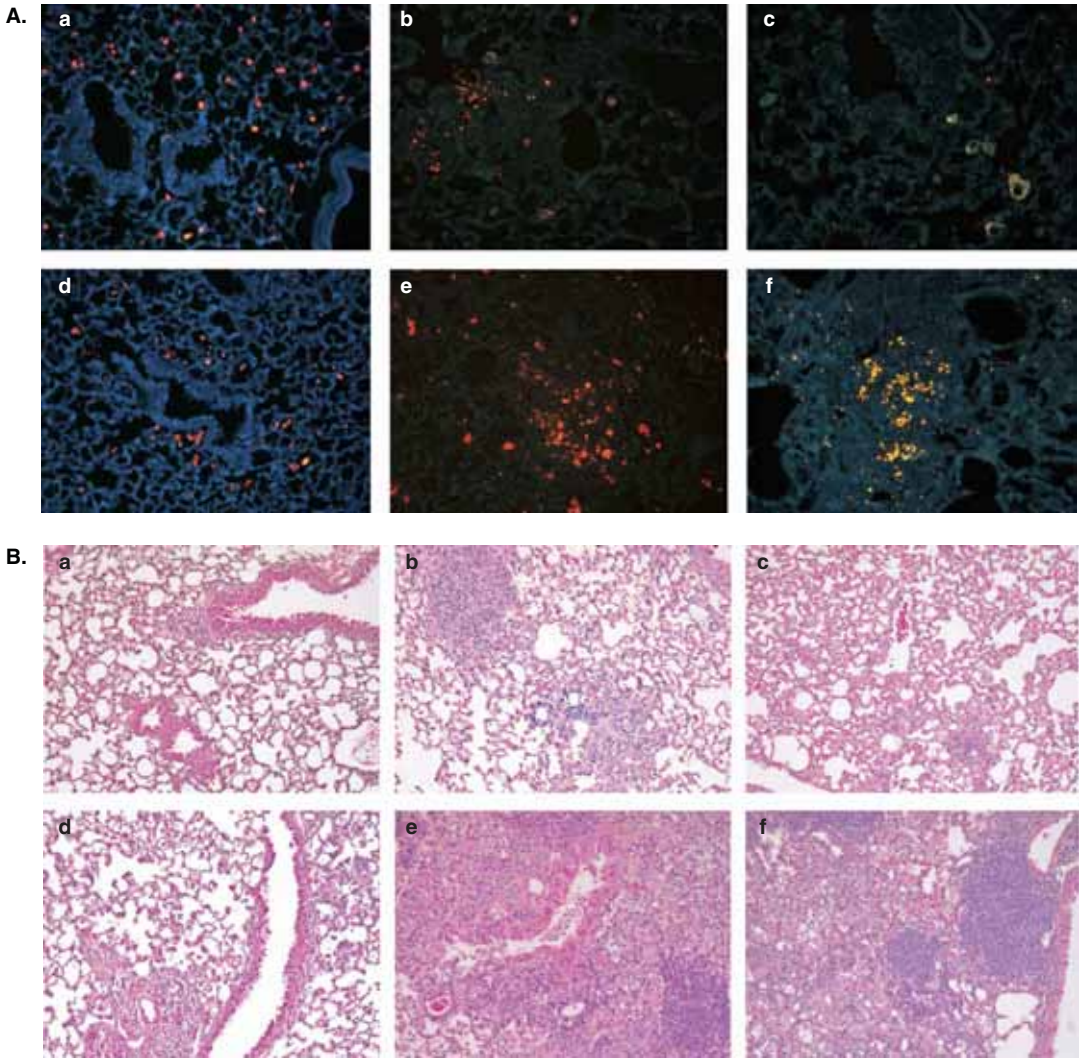

Figure 4. Effects of nanoparticles on lung morphology. A. Localisation of QD705-PEG and QD705-COOH in the lungs of mice, detected as red fluorescence via fluorescence microscopy (X100). QD705-PEG on day 2 (a), day 17 (b), day 90 (c), and QD705-COOH on day 2 (d), day 17 (e), day 90 (f). B. Haematoxylin- and eosin-stained lung sections (X100). QD705-PEG day 2 (a), day 17 (b), day 90 (c), and QD705-COOH day 2 (d), day 17 (e), day 90 (f).

safety needs to be evaluated. Recently we demonstrated that intravenous injection of a single dose of QD705 caused delayed adverse responses in the liver of mice (Lin et al. 2011). Here we evaluated the biological responses to intratracheal instillation of a single dose of QD705 in the lung of mice. In the present study, we showed that intratracheal instillation of QD705 caused adverse responses in the lungs of mice and PEG coating failed to prevent these effects. This study demonstrated three important phenomena: (1) QD705-COOH persistently induced acute neutrophil infiltration, interstitial lymphocyte infiltration and a granulomatous reaction from days 17 to 90 post-treatment, but the QD-PEG-induced granulomatous reaction disappeared on day 90 post-treatment; (2) Both QD705-PEG and QD705-COOH induced gene expression of pro-inflammatory cytokines, tissue remodelling and chemokines in lung tissues and transiently reduced pulmonary function on day 17 post-treatment; and (3) Because nano-TiO_2 and nano-SiO_2 with similar shape and size failed to induce granulomatous reactions at doses much higher than the doses of QD705, the shape and size of nanoparticles are not major factors for pulmonary granulomatous reaction.

Table III. Effects of QD705-PEG and QD705-COOH on pulmonary function on day 17.

	Control	QD705-PEG	Control	QD705-COOH
Forced vital capacity (FVC)	1.35 ± 0.21	0.99 ± 0.28*	1.31 ± 0.08	0.91 ± 0.16*
Forced expiratory volume (FEV100)	1.35 ± 0.20	1.00 ± 0.26*	1.20 ± 0.12	0.83 ± 0.19*
Vital capacity (VC)	1.38 ± 0.24	1.05 ± 0.27*	1.40 ± 0.09	0.99 ± 0.15*
Forced expiratory flow (FEF)	74.32 ± 18.96	38.31 ± 11.11*	69.18 ± 15.42	48.76 ± 23.19*
Peak expiratory Flow (PEF)	20.58 ± 0.92	20.04 ± 1.81	18.24 ± 6.36	18.78 ± 4.81

Mice were injected with a single dose of 60-μg QD705-PEG and QD705-COOH and sacrificed on day 17. Parameters of pulmonary function were measured with a forced pulmonary manoeuvre system immediately before sacrifice. Each value represents the mean ± SD of eight mice. *$p < 0.05$ compared with the vehicle-treated group.

Table IV. Effects of nanoparticle exposure on gene expression in the lung.

	QD705-PEG				QD705-COOH				TiO_2	SiO_2
	2 days	17 days		90 days	2 days	17 days		90 days	17 days	17 days
	60 μg	12 μg	60 μg	60 μg	60 μg	12 μg	60 μg	60 μg	500 μg	100 μg
Pro-inflammatory cytokines										
TNF-α	1.5 ± 0.5*	2.2 ± 0.5*	2.9 ± 0.7*	2.6 ± 0.9*	2.2 ± 0.8*	2.7 ± 0.9*	4.9 ± 3.3*	2.2 ± 0.8*	1.3 ± 0.4*	1.1 ± 0.2
IL-1β	1.0 ± 0.2	1.7 ± 0.4*	1.6 ± 0.2*	1.1 ± 0.5	2.0 ± 0.8*	1.6 ± 0.2*	3.0 ± 1.0*	1.0 ± 0.4	0.7 ± 0.2*	1.0 ± 0.3
IL-6	1.7 ± 0.2*	3.5 ± 1.8*	6.5 ± 3.1*	0.7 ± 0.4*	3.5 ± 1.5*	1.7 ± 0.7*	4.8 ± 3.3*	0.6 ± 0.4*	0.7 ± 0.3	1.0 ± 0.3
CXCL1(KC)	1.2 ± 0.4	3.1 ± 1.6*	10.5 ± 5.9*	5.1 ± 2.2*	3.2 ± 1.4*	4.8 ± 2.9*	6.7 ± 2.9*	3.6 ± 1.8*	0.9 ± 0.4	1.2 ± 0.6
CCL2 (MCP-1)	2.1 ± 0.9*	5.5 ± 3.0*	12.7 ± 5.9*	3.9 ± 1.8*	8.3 ± 3.3*	6.9 ± 4.0*	18.7 ± 11.5*	3.4 ± 1.6*	0.8 ± 0.3	0.9 ± 0.3
Tissue remodelling genes										
IL-10	1.0 ± 0.4	2.1 ± 1.0*	2.2 ± 0.9*	1.8 ± 0.6*	1.0 ± 0.3	3.1 ± 1.9*	7.4 ± 4.5*	3.3 ± 1.3*	1.6 ± 0.8*	1.4 ± 0.4*
IL-13	1.1 ± 0.4	2.9 ± 1.3*	3.3 ± 1.6*	0.8 ± 0.2	1.5 ± 0.5*	3.4 ± 1.8*	2.5 ± 1.2*	0.9 ± 0.4	1.4 ± 0.4*	1.0 ± 0.2
MMP12	3.9 ± 2.0*	3.4 ± 1.5*	12.0 ± 5.7*	2.4 ± 1.1*	7.1 ± 3.0*	4.4 ± 2.8*	16.4 ± 10.4*	3.1 ± 1.3*	1.1 ± 0.2	1.3 ± 0.4
Chemokines										
CCL1	3.9 ± 2.0*	5.4 ± 1.9*	12.0 ± 5.7*	2.4 ± 1.1*	7.1 ± 3.0*	11.3 ± 4.5*	16.4 ± 10.4*	3.1 ± 1.3*	0.7 ± 0.3*	0.8 ± 0.4
CCL17	1.3 ± 0.1*	2.9 ± 1.4*	5.4 ± 0.8*	3.7 ± 1.0*	1.4 ± 0.3*	2.9 ± 1.2*	3.2 ± 2.3*	3.3 ± 0.5*	1.1 ± 0.3	1.7 ± 0.8*
CXCL13	1.0 ± 0.4	1.2 ± 0.3*	4.4 ± 1.8*	1.0 ± 0.5	0.9 ± 0.1	3.3 ± 1.4*	3.8 ± 2.4*	3.1 ± 1.2*	1.0 ± 0.3	2.3 ± 1.3*

Mice were given a single dose of nanoparticles via intratracheal instillation and sacrificed 2, 17 or 90 days after dosing. The relative mRNA levels of specific gene expression in the lung were quantified by real-time PCR. Data are represented as fold change from vehicle-treated mice.*$p < 0.05$ as compared with the vehicle-treated group.

However, the chemical composition of nanoparticles might be one of the major factors for these adverse responses in our present study.

Our results suggest that a variety of cell types are involved in the QD705-induced granulomatous reaction with a time sequence (Figure 5). The pathological changes start with acute necrotising inflammation in some bronchioles and the formation of QD705-loaded foamy-like macrophages in the alveolar spaces on day 2, whereas there is no significant granuloma formation. Then, pulmonary granulomas appear in the peribronchiolar areas and interstitium on day 17. QD705-induced granulomas are composed mainly of macrophages and are mixed with lymphocytes, neutrophils and other inflammatory cells. Macrophages function as antigen-presenting cells for T-cell activation and activated T cells are involved in initiation and regulation of granuloma formation (Kaufmann and Ladel 1994). It is likely that the triggered stimulus is QD705 and alveolar macrophages initiate a tissue reaction through phagocytosis of QD705, followed by the release of a variety of cytokines and chemokines to recruit

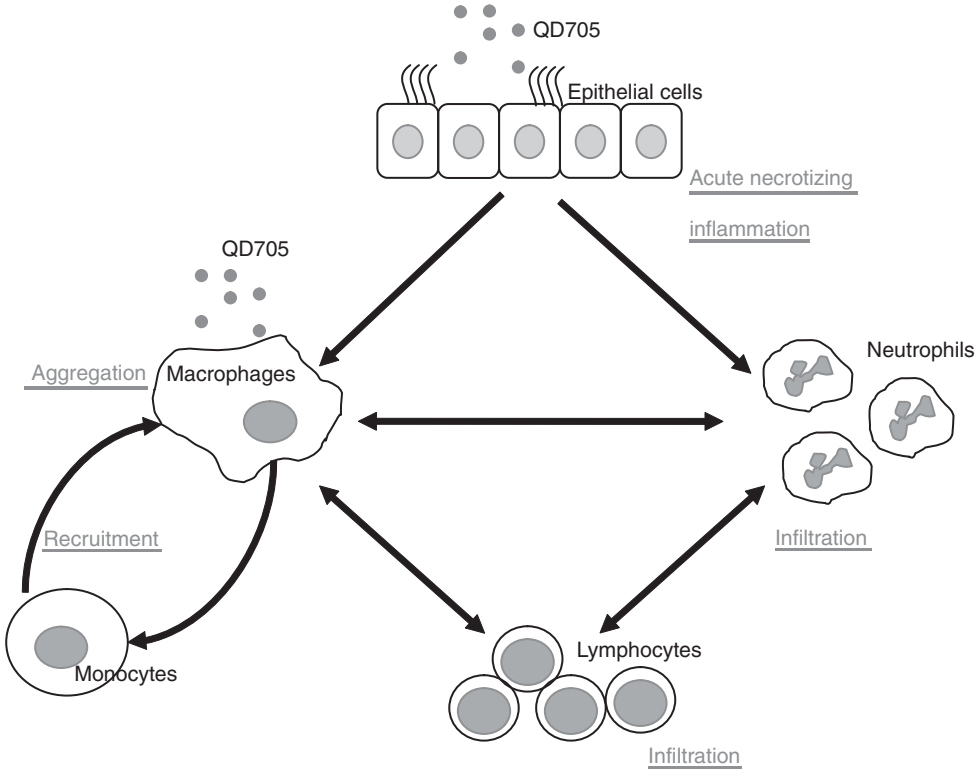

Figure 5. Proposed cell interactions in the QD705-induced granulomatous reaction in the lung.

different immune cells and consequently granuloma are formed.

Other studies showed that carbon nanotubes and nano-TiO_2 also induced pulmonary granuloma formation. Intratracheal instillation of 0.5-mg single-walled carbon nanotubes induced granulomas and interstitial inflammation in mice on day 7 (Lam et al. 2004). More recently, Park et al. (2009) demonstrated that intratracheal instillation of 0.6 mg of 20 nm nano-TiO_2 induced granulomas in mice on day 14. However, we failed to observe that 0.5 mg (6.25 mol) nano-TiO_2 or 0.1 mg (1.66 mol) nano-SiO_2 induced a granulomatous reaction in our present study. However, intratracheal instillation of 60 μg (40 pmol) of QD705-PEG and QD705-COOH induced granuloma formation on day 17. These findings imply that QD705 could induce more severe pulmonary toxicity than other engineered nanoparticles at the same dose.

Pulmonary function parameters are essential for assessing the health condition of the lungs in humans. However, there is little information available on the effects of nanoparticles on pulmonary function. In the present study, we found that intratracheal instillation of QD705 significantly reduced the FVC, FEV100, VC and FEF25–75, suggesting an obstructive dysfunction of the lung. In an obstructive condition, the airways of the lungs become narrow or are blocked so that one cannot exhale completely, compatible with the histopathology of QD705-induced granulomas around the peribronchiolar areas. Chronic obstructive pulmonary diseases are considered obstructive lung diseases (Ferrara 2011), but interstitial granulomas in the present study usually indicate a member of restrictive lung diseases. Pulmonary function, however, showed a different response to challenge with QD705. One possible explanation is that QD705-induced tissue reaction causes the effect of narrowed or blocked airways greater than pulmonary interstitial granulomas do.

The QD705-induced expression of many cytokines and chemokines (Table IV) may play an important role in the neutrophil and lymphocyte infiltration and granulomatous reaction in this study. Granulomatous lung diseases, such as sarcoidosis, hypersensitivity pneumonitis and chronic beryllium disease, cause morbidity and mortality worldwide (Chen and Moller 2007). Pro-inflammatory cytokines or chemokines, such as TNF-α (Pejnovic et al. 1994), IL-1 (Denis, Bedard et al. 1993), IL-6 (Pejnovic et al. 1994; Schuyler et al. 2000), MCP-1(CCL2) (Girard et al. 2004) and IL-8 (Fujimori et al. 2003) are released from patients with granulomatous lung diseases. MCP-1 is an important chemokine in pathological conditions involving monocyte/macrophage infiltration (Hasegawa et al. 1999). The roles of CCL1 and CCL17 in immune responses are only beginning to be delineated, yet several recent reports indicate that these chemokines play important roles in T cell activation (Henry et al. 2008). In line with the pathology, we assume that these key cytokines and chemokines might play important roles in QD705-induced inflammatory responses and could also be involved in the pathogenesis of pulmonary granulomas. Erdely et al. (2009) reported that pulmonary exposure to multi-walled carbon nanotubes induced granuloma formation and triggered the induction of primary cytokines such as IL-1β, IL-6 and IL-1β, as well as inflammatory mediators, chemokines (MCP-1). Park et al. (2009) found that inflammation-related genes including CXCL1, CCL2 and MMP-12 also markedly increased in nano-TiO_2-induced pulmonary granuloma formation. Macrophage metalloelastase is a MMP-12 capable of degrading extracellular matrix components such as elastin and is involved in tissue remodelling processes in pulmonary inflammatory diseases (Nenan et al. 2005). IL-10 knockout mice accumulated more inflammatory cells in their BALF and had greater histological evidence of inflammation and granuloma formation than did wild-type mice (Gudmundsson et al. 1998). These findings suggest that QD705 persistently induced inflammation and remodelling in the lung.

Based on our results, we suggest that cadmium-based QD705, even those with PEG coating, are not good carriers for pulmonary delivery of drugs or pulmonary imaging. However, we do not know what physicochemical properties of QD705, such as chemical components, surface area, charge or biological half-life, contribute to these adverse responses. More experiments are needed to compare the effects of different physicochemical properties of QDs on granuloma formation. Since macrophages and epithelial cells may be the primary targets, some *in vitro* models may be applied to screen for optimal physicochemical properties before animal studies. Indeed, our *in vitro* experiments showed that QD705 was more cytotoxic than TiO_2 and SiO_2, which was consistent with the results of our *in vivo* studies. Furthermore, both QD705-PEG and QD705-COOH at the highest doses were cytotoxic to macrophage J774A.1 cells, and both induced pulmonary granulomas.

Acknowledgements

This work was supported by a research grant, 99A1-NM-PP08-007 from the Center of Nanomedicine Research and the Division of Environmental Health and Occupational Medicine of the National Health Research Institutes, Taiwan, ROC.

Declaration of interest

The authors report no conflicts of interest. The authors alone are responsible for the content and writing of the paper.

References

Ballou B, Lagerholm BC, Ernst LA, Bruchez MP, Waggoner AS. 2004. Noninvasive imaging of quantum dots in mice. Bioconjug Chem 15:79–86.

Chan WH, Shiao NH, Lu PZ. 2006. CdSe quantum dots induce apoptosis in human neuroblastoma cells via mitochondrial-dependent pathways and inhibition of survival signals. Toxicol Lett 167:191–200.

Chang E, Thekkek N, Yu WW, Colvin VL, Drezek R. 2006. Evaluation of quantum dot cytotoxicity based on intracellular uptake. Small 2:1412–1417.

Chen AA, Derfus AM, Khetani SR, Bhatia SN. 2005. Quantum dots to monitor RNAi delivery and improve gene silencing. Nucleic Acids Res 33:e190.

Chen ES, Moller DR. 2007. Expression profiling in granulomatous lung disease. Proc Am Thorac Soc 4:101–107.

Dabbousi BO, Rodriguez-Viejo J, Mikulec FV, Heine JR, Mattoussi H, Ober R, et al. 1997. (CdSe)ZnS core-shell quantum dots: Synthesis and characterization of a size series of highly luminescent nanocrystallites. J Phys Chem 101:9463–9475.

Denis M, Bedard M, Laviolette M, Cormier Y. 1993. A study of monokine release and natural killer activity in the bronchoalveolar lavage of subjects with farmer's lung. Am Rev Respir Dis 147:934–939.

Deng Z, Schulz O, Lin S, Ding B, Liu X, Wei X, et al. 2010. Aqueous synthesis of zinc blende CdTe/CdS magic-core/thick-shell tetrahedral-shaped nanocrystals with emission tunable to near-infrared. J Am Chem Soc 132:5592–5593.

Erdely A, Hulderman T, Salmen R, Liston A, Zeidler-Erdely PC, Schwegler-Berry D, et al. 2009. Cross-talk between lung and systemic circulation during carbon nanotube respiratory exposure. Potential biomarkers. Nano Lett 9:36–43.

Ferrara A2011. Chronic obstructive pulmonary disease. Radiol Technol 82:245–263.

Fujimori Y, Kataoka M, Tada S, Takehara H, Matsuo K, Miyake T, et al. 2003. The role of interleukin-8 in interstitial pneumonia. Respirology 8:33–40.

Gao X, Cui Y, Levenson RM, Chung LW, Nie S. 2004. In vivo cancer targeting and imaging with semiconductor quantum dots. Nat Biotechnol 22:969–976.

Gao X, Dave SR. 2007. Quantum dots for cancer molecular imaging. Adv Exp Med Biol 620:57–73.

Gao X, Wang T, Wu B, Chen J, Yue Y, Dai N, et al. 2008. Quantum dots for tracking cellular transport of lectin-functionalized nanoparticles. Biochem Biophys Res Commun 377:35–40.

Gaspar MM, Gobbo O, Ehrhardt C. 2010. Generation of liposome aerosols with the Aeroneb Pro and the AeroProbe nebulizers. J Liposome Res 20:55–61.

Girard M, Israel-Assayag E, Cormier Y. 2004. Pathogenesis of hypersensitivity pneumonitis. Curr Opin Allergy Clin Immunol 4:93–98.

Gudmundsson G, Bosch A, Davidson BL, Berg DJ, Hunninghake GW. 1998. Interleukin-10 modulates the severity of hypersensitivity pneumonitis in mice. Am J Respir Cell Mol Biol 19:812–818.

Hasegawa M, Sato S, Takehara K. 1999. Augmented production of chemokines (monocyte chemotactic protein-1 (MCP-1), macrophage inflammatory protein-1alpha (MIP-1alpha) and MIP-1beta) in patients with systemic sclerosis: MCP-1 and MIP-1alpha may be involved in the development of pulmonary fibrosis. Clin Exp Immunol 117:159–165.

Hauck TS, Anderson RE, Fischer HC, Newbigging S, Chan WC. 2010. In vivo quantum-dot toxicity assessment. Small 6:138–144.

Henry CJ, Ornelles DA, Mitchell LM, Brzoza-Lewis KL, Hiltbold EM. 2008. IL-12 produced by dendritic cells augments CD8+ T cell activation through the production of the chemokines CCL1 and CCL17. J Immunol 181:8576–8584.

Jia N, Lian Q, Shen H, Wang C, Li X, Yang Z. 2007. Intracellular delivery of quantum dots tagged antisense oligodeoxynucleotides by functionalized multiwalled carbon nanotubes. Nano Lett 7:2976–2980.

Karathanasis E, Ayyagari AL, Bhavane R, Bellamkonda RV, Annapragada AV. 2005. Preparation of in vivo cleavable agglomerated liposomes suitable for modulated pulmonary drug delivery. J Control Release 103:159–175.

Kaufmann SH, Ladel CH. 1994. Role of T cell subsets in immunity against intracellular bacteria: experimental infections of knock-out mice with Listeria monocytogenes and Mycobacterium bovis BCG. Immunobiology 191:509–519.

Lam CW, James JT, McCluskey R, Hunter RL. 2004. Pulmonary toxicity of single-wall carbon nanotubes in mice 7 and 90 days after intratracheal instillation. Toxicol Sci 77:126–134.

Legler DF, Loetscher M, Roos RS, Clark-Lewis I, Baggiolini M, Moser B. 1998. B cell-attracting chemokine 1, a human CXC chemokine expressed in lymphoid tissues, selectively attracts B lymphocytes via BLR1/CXCR5. J Exp Med 187:655–660.

Lin CH, Yang MH, Chang LW, Yang CS, Chang H, Chang WH, et al. 2011. Cd/Se/Te-based quantum dot 705 modulated redox homeostasis with hepatotoxicity in mice. Nanotoxicology. Posted online on December 10, 2010. (doi:10.3109/17435390.2010.539712)

Lin P, Chen JW, Chang LW, Wu JP, Redding L, Chang H, et al. 2008. Computational and ultrastructural toxicology of a nanoparticle, Quantum Dot 705, in mice. Environ Sci Technol 42:6264–6270.

Liu J, Gong T, Fu H, Wang C, Wang X, Chen Q, et al. 2008. Solid lipid nanoparticles for pulmonary delivery of insulin. Int J Pharm 356:333–344.

Lovric J, Cho SJ, Winnik FM, Maysinger D. 2005. Unmodified cadmium telluride quantum dots induce reactive oxygen species formation leading to multiple organelle damage and cell death. Chem Biol 12:1227–1234.

Mahto SK, Park C, Yoon TH, Rhee SW. 2010. Assessment of cytocompatibility of surface-modified CdSe/ZnSe quantum dots for BALB/3T3 fibroblast cells. Toxicol In Vitro 24:1070–1077.

Manabe N, Hoshino A, Liang YQ, Goto T, Kato N, Yamamoto K2006. Quantum dot as a drug tracer in vivo. IEEE Trans Nanobioscience 5:263–267.

Mansour HM, Rhee YS, Wu X. 2009. Nanomedicine in pulmonary delivery. Int J Nanomedicine 4:299–319.

Meldrum DR, Meng X, Sheridan BC, McIntyre RC Jr, Harken AH, Banerjee A. 1998. Tissue-specific protein kinase C isoforms differentially mediate macrophage TNFalpha and IL-1beta production. Shock 9:256–260.

Monteiro-Riviere NA, Inman AO, Zhang LW. 2009. Limitations and relative utility of screening assays to assess engineered nanoparticle toxicity in a human cell line. Toxicol Appl Pharmacol 234: 222–235.

Mulder WJ, Strijkers GJ, Nicolay K, Griffioen AW. 2010. Quantum dots for multimodal molecular imaging of angiogenesis. Angiogenesis 13:131–134.

Nakayama T, Hieshima K, Nagakubo D, Sato E, Nakayama M, Kawa K, et al. 2004. Selective induction of Th2-attracting chemokines CCL17 and CCL22 in human B cells by latent membrane protein 1 of Epstein-Barr virus. J Virol 78:1665–1674.

Nathan N, Denizot Y. 1998. Anti-inflammatory cytokines (IL-4, IL-10, IL-13) in plasma during mesenteric infarction. Mediators Inflamm 7:119.

Nenan S, Boichot E, Lagente V, Bertrand CP. 2005. Macrophage elastase (MMP-12): a pro-inflammatory mediator? Mem Inst Oswaldo Cruz 100(Suppl 1):167–172.

Obonyo O, Fisher E, Edwards M, Douroumis D. 2010. Quantum dots synthesis and biological applications as imaging and drug delivery systems. Crit Rev Biotechnol 30:283–301.

Park EJ, Yoon J, Choi K, Yi J, Park K. 2009. Induction of chronic inflammation in mice treated with titanium dioxide nanoparticles by intratracheal instillation. Toxicology 260:37–46.

Pejnovic N, Tomic O, Vojvodic D, Djordjevic N, Jovicic Z, Kukic Z, et al. 1994. IL-1, TNF and IL-6 production by alveolar mononuclear cells in patients with sarcoidosis. Srp Arh Celok Lek 122(Suppl 1):96–97.

Qi L, Gao X2008. Emerging application of quantum dots for drug delivery and therapy. Expert Opin Drug Deliv 5:263–267.

Ryman-Rasmussen JP, Riviere JE, Monteiro-Riviere NA. 2006. Penetration of intact skin by quantum dots with diverse physicochemical properties. Toxicol Sci 91:159–165.

Schuyler M, Gott K, Cherne A. 2000. Mediators of hypersensitivity pneumonitis. J Lab Clin Med 136:29–38.

Veronese FM, Pasut G. 2005. PEGylation, successful approach to drug delivery. Drug Discov Today 10:1451–1458.

Xing Y, Smith AM, Agrawal A, Ruan G, Nie S. 2006. Molecular profiling of single cancer cells and clinical tissue specimens with semiconductor quantum dots. Int J Nanomedicine 1:473–481.

Zhang H, Yee D, Wang C. 2008. Quantum dots for cancer diagnosis and therapy: biological and clinical perspectives. Nanomedicine (Lond) 3:83–91.

Zhang Y, Zhu J, Tang Y, Chen X, Yang Y. 2009. The preparation and application of pulmonary surfactant nanoparticles as absorption enhancers in insulin dry powder delivery. Drug Dev Ind Pharm 35:1059–1065.